Original Article

Three-dimensional ultrashort echo time magnetic resonance imaging in assessment of idiopathic pulmonary fibrosis, in comparison with high-resolution computed tomography

Xiaoyan Yang[1,2], Min Liu[3], Jianghui Duan[3], Haishuang Sun[2], Jing An[4], Thomas Benkert[5], Huaping Dai[1,2], Chen Wang[1,2,6]

[1]Department of Pulmonary and Critical Care Medicine, China-Japan Friendship Hospital, Capital Medical University, Beijing, China; [2]National Center for Respiratory Medicine, Institute of Respiratory Medicine, Chinese Academy of Medical Sciences, National Clinical Research Center for Respiratory Diseases, Beijing, China; [3]Department of Radiology, China-Japan Friendship Hospital, Beijing, China; [4]Siemens Shenzhen Magnetic Resonance Ltd., Shenzhen, China; [5]MR Application Predevelopment, Siemens Healthcare GmbH, Erlangen, Germany; [6]Chinese Academy of Medical Sciences and Peking Union Medical College, Beijing, China

Contributions: (I) Conception and design: M Liu, H Dai, C Wang; (II) Administrative support: M Liu, H Dai; (III) Provision of study materials or patients: X Yang, H Sun, H Dai, C Wang; (IV) Collection and assembly of data: X Yang, J Duan, M Liu; (V) Data analysis and interpretation: X Yang, M Liu, J An, T Benkert; (VI) Manuscript writing: All authors; (VII) Final approval of manuscript: All authors.

Correspondence to: Min Liu. Department of Radiology, China-Japan Friendship Hospital, 2 Yinghua Dong Street, Hepingli, Chaoyang District, Beijing 100029, China. Email: mike0763@126.com; Huaping Dai. Department of Pulmonary and Critical Care Medicine, China-Japan Friendship Hospital, 2 Yinghua Dong Street, Hepingli, Chaoyang District, Beijing 100029, China. Email: daihuaping@ccmu.edu.cn; Chen Wang. Department of Pulmonary and Critical Care Medicine, China-Japan Friendship Hospital, 2 Yinghua Dong Street, Hepingli, Chaoyang District, Beijing 100029, China. Email: cyh-birm@263.net.

Background: We aimed to evaluate the image quality, feasibility, and diagnostic performance of three-dimensional ultrashort echo time magnetic resonance imaging (3D UTE-MRI) to assess idiopathic pulmonary fibrosis (IPF) compared with high-resolution computed tomography (HRCT) and half-Fourier single-shot turbo spin-echo (HASTE) MRI.

Methods: A total of 36 patients with IPF (34 men; mean age: 62±8 years, age range: 43 to 78 years) were prospectively included and underwent HRCT and chest MRI on the same day. Chest MRI was performed with a free-breathing 3D spiral UTE pulse sequence and HASTE sequence on a 1.5 T MRI. Two radiologists independently evaluated the image quality of the HRCT, HASTE, and 3D UTE-MRI. They assessed the representative imaging features of IPF, including honeycombing, reticulation, traction bronchiectasis, and ground-glass opacities. Image quality of the 3D UTE-MRI, HASTE, and HRCT were assessed using a 5-point visual scoring method. Kappa and weighted kappa analysis were used to measure intra- and inter-observer and inter-method agreements. Sensitivity (SE), specificity (SP), and accuracy (AC) were used to assess the performance of 3D UTE-MRI for detecting image features of IPF and monitoring the extent of pulmonary fibrosis. Linear regressions and Bland-Altman plots were generated to assess the correlation and agreement between the assessment of the extent of pulmonary fibrosis made by the 2 observers.

Results: The image quality of HRCT was higher than that of HASTE and UTE-MRI (HRCT *vs.* UTE-MRI *vs.* HASTE: 4.9±0.3 *vs.* 4.1±0.7 *vs.* 3.0±0.3; P<0.001). Interobserver agreement of HRCT, HASTE, and 3D UTE-MRI when assessing pulmonary fibrosis was substantial and excellent (HRCT: 0.727≤ κ ≤1, P<0.001; HASTE: 0.654≤ κ ≤1, P<0.001; 3D UTE-MRI: 0.719≤ κ ≤0.824, P<0.001). In addition, reticulation (SE: 97.1%; SP: 100%; AC: 97.2%; κ =0.654), honeycombing (SE: 83.3%; SP: 100%; AC: 86.1%; κ =0.625) patterns, and traction bronchiectasis (SE: 94.1%; SP: 100%; AC: 94.4%, κ =0.640) were also well-visualized on 3D UTE-MRI, which was significantly superior to HASTE. Compared with HRCT, the sensitivity of 3D UTE-MRI to detect signs of pulmonary fibrosis (n=35) was 97.2%. The interobserver agreement in

elevation of the extent of pulmonary fibrosis with HRCT and 3D UTE-MRI was R^2=0.84 (P<0.001) and R^2=0.84 (P<0.001), respectively. The extent of pulmonary fibrosis assessed with 3D UTE-MRI [median =9, interquartile range (IQR): 6.25 to 10.00] was lower than that from HRCT (median =12, IQR: 9.25 to 13.00; U=320.00, P<0.001); however, they had a positive correlation (R=0.72, P<0.001).

Conclusions: As a radiation-free non-contrast enhanced imaging method, although the image quality of 3D UTE-MRI is inferior to that of HRCT, it has high reproducibility to identify the imaging features of IPF and evaluate the extent of pulmonary fibrosis.

Keywords: Lungs; three-dimensional ultrashort echo time magnetic resonance imaging (3D UTE-MRI); high-resolution computed tomography (HRCT); idiopathic pulmonary fibrosis (IPF)

Submitted Nov 25, 2021. Accepted for publication May 27, 2022.
doi: 10.21037/qims-21-1133
View this article at: https://dx.doi.org/10.21037/qims-21-1133

Introduction

Idiopathic pulmonary fibrosis (IPF) is a chronic, progressive, fibrosing disease of the lung with a poor prognosis. The median survival of IPF is 3–5 years from diagnosis (1). High-resolution computed tomography (HRCT) plays a key role in diagnosing and evaluating IPF (1). However, radiation exposure is a concern for patients with IPF who require multiple HRCT scans during routine follow-up. Thus, a radiation-free imaging method is desirable for patients with IPF.

Pulmonary magnetic resonance imaging (MRI) is an imaging modality that does not use ionizing radiation, which has progressed significantly in the past decade (2). The single-shot fast spin-echo [half-Fourier single-shot turbo spin-echo (HASTE)] and two-dimensional balanced steady-state free-precession (bSSFP) sequences are used to evaluate the morphologic details of interstitial lung disease (ILD) and have demonstrated moderate agreement with findings based on HRCT (3-7). Although the bSSFP sequence is less valuable in depicting minor fibrotic changes, the diagnostic accuracy of MRI tends to increase in more advanced ILD stages (7). The ILD signal intensity volume (ISIV) on T2-BLADE can assess the volumetric extent of abnormal interstitial lung signal intensity modifications in patients with IPF in a reproducible manner (8). Recently, the value of ultrashort echo time MRI (UTE-MRI) of the lung has been demonstrated in imaging lungs and lung diseases, providing high signal-to-noise rations (SNRs) and high-resolution images for the quantitative and qualitative assessment of changes in lung parenchyma (9-16). However, there is limited research about UTE-MRI in the assessment of lung abnormalities found in ILD (17-19). Therefore, the objective of this study was to evaluate the image quality, feasibility, and diagnostic performance of 3D UTE-MRI in the assessment of IPF, compared with HRCT and HASTE. We present the following article in accordance with the GRRAS reporting checklist (available at https://qims.amegroups.com/article/view/10.21037/qims-21-1133/rc).

Methods

Patients

The study was approved by the Ethics Committee of the China-Japan Friendship Hospital (No. 2019-123-K85-1). The study was conducted in accordance with the Declaration of Helsinki (as revised in 2013). All study participants provided written informed consent. From August 2020 to July 2021, patients with a definitive diagnosis of IPF were prospectively enrolled and diagnosed by the multidisciplinary diagnostic team based on the 2018 American Thoracic Society, European Respiratory Society, Japanese Respiratory Society, and Latin American Thoracic Association (ATS/ERS/JRS/ALAT) criteria (1). All patients who underwent HRCT and MRI on the same day were included. The exclusion criteria were as follows: (I) participants with other pulmonary diseases, such as lung cancer or another malignancy; (II) participants with long-term oxygen therapy; (III) participants with MRI contraindications, such as a pacemaker or claustrophobia; and (IV) participants who rejected the MRI examination.

HRCT scan

All patients underwent HRCT using multidetector CT

(MDCT) systems (Lightspeed VCT/64, GE Healthcare, Chicago, IL, USA; Toshiba Aquilion ONE TSX-301C/320, Toshiba, Tochigi, Japan; Philips iCT/256, Philips, Amsterdam, Netherlands). During a single breath-hold, we craniocaudally scanned the whole chest of each participant from the lung apex to the lowest hemidiaphragm. Acquisition parameters and reconstruction parameters were in accordance with CT standards: tube voltage of 100–120 kV, tube current of 100–300 mAs, section thickness of 0.625–1 mm, table speed of 39.37 mm/s, gantry rotation time of 0.8 s, and reconstruction increment of 1–1.25 mm. All participants assumed a supine position with their hands raised above their heads to undertake the scan.

MRI image acquisition

All participants underwent a chest MRI on a 1.5T MRI scanner (MAGNETOM Aera; Siemens Healthcare, Erlangen, Germany) with an 18-channel phased-array body coil and 12-channel spine coil. The 3D UTE, a prototypic 3D volumetric interpolated breath-hold examination (VIBE) sequence with a stack-of spirals trajectory, was used for data acquisition as described in a previous study (20). The sequence was implemented at end-expiration during free-breathing with the following key parameters: coronal acquisition plane; repetition time =3.85 ms; echo time =0.05 ms; flip angle =5°; field of view (FOV) =480×480 mm^2; in-plane resolution =1.5 mm × 1.5 mm; spiral interleaves =240; slice thickness =1.5 mm, slice per slab =160; and spiral readout duration =1,800 μs. A non-uniform Fourier Transform (NUFT) was used for image reconstructions (21). Prospective respiratory gating without navigator positioning was used to minimize motion artifacts, and the specified coil element closest to the diaphragm edge was selected for navigator signal processing. The gating tolerance was 40% (22). The acquisition times varied from 6 to 7 min, depending on the respiration pattern of individual patients. The HASTE was implemented during the breath-hold with the following key parameters: axial and coronal acquisition plane; repetition time =868 ms; echo time =46 ms; flip angle =160°; FOV =340×340 mm^2; voxel size =1.3 mm × 1.3 mm × 8 mm. Image reconstructions were performed with a half-Fourier method using k-space symmetry. Electrocardiogram (ECG) triggering was used to minimize motion artifacts. The acquisition time was 16 seconds.

Image analysis

Coronal images of HRCT and transversal images of 3D UTE-MRI were reconstructed. The HRCT and MRI images were evaluated by 2 chest radiologists with 15 years of experience (reader 1) and 8 years of experience (reader 2) in the Picture Archiving and Communications System; the radiologists were blinded to patient information and data. Two readers independently evaluated all HRCT images at the lung [level: −550 Hounsfiled units (HU), width: 1,600 HU] window settings. To evaluate intra-observer agreement, reader 2 evaluated the 3D UTE-MR images a second time after one month.

Image quality analysis

To evaluate the image quality 3D UTE-MRI, HASTE, and HRCT, a 5-point visual scoring method (17) was adopted (1, nondiagnostic image quality; 2, poor image quality; 3, acceptable image quality; 4, good imaging quality; 5, excellent image quality). The 5-point visual score referenced the Likert scale as previously described (10) (1, images with severe artifacts; 2, obscure lung anatomy with moderate artifacts; 3, mild artifacts present but they do not obscure lung anatomy; 4, minimal artifacts but with good bronchi and vessel visibility; 5, no artifacts present and good bronchi and vessel visibility). Two radiologists independently supplied the visual score to analyze the interobserver agreement of image quality. To compare the imaging quality of HRCT, UTE, and HASTE, the final scores of each method were obtained via consensus of the 2 radiologists.

Feature-based image analysis

We compared the representative imaging features of ILDs, including honeycombing, reticulation, traction bronchiectasis, and ground-glass opacities (GGO), among 3D UTE, HASTE, and HRCT using a 2-point visual scoring method (0, absent; 1, present) (23,24). According to Müller *et al.* (25), GGO on MRI was defined as an area of increased signal intensity without obscuration of the pulmonary vessels. In cases of discrepancy between the observers regarding the detection of abnormalities, a final interpretation was obtained by consensus from 2 radiologists.

The extent of pulmonary interstitial fibrosis was graded

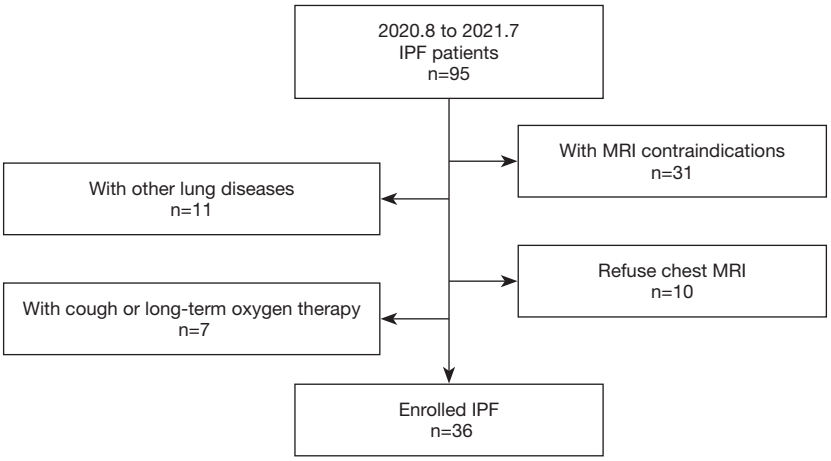

Figure 1 The flowchart of inclusion and exclusion criteria of patients in this study. IPF, idiopathic pulmonary fibrosis; MRI, magnetic resonance imaging.

with a system used by Gay *et al.* (23). Each lung was divided into the following three zones: the upper zones, defined as the area above the aortic arch; the middle zone, defined as the area between the aortic arch and the pulmonary veins; and the lower zone, defined as the area below the pulmonary veins (26). The sum of the scores for all zones was obtained for each patient (minimum score, 0; maximum score, 30).

Statistical analysis

Statistical analyses were performed with the software SPSS 23.0 (IBM Corp., Armonk, NY, USA). Continuous values were presented as means ± standard deviations (SD) or the median with interquartile range (IQR). The Wilcoxon-rank sum test was used to compare image quality scores among the 3D UTE-MRI, HRCT, and HASTE images. Using HRCT as the reference standard, the ability of 3D UTE-MRI to display features of interstitial fibrosis was assessed using sensitivity (SE), specificity (SP), and accuracy (AC). Kappa and weighted kappa values were used to determine intra-observer agreement and interobserver agreement. The intra-observer, inter-observer, and inter-method agreements were determined as excellent for kappa =0.8–1.0, substantial for kappa =0.6–0.8, moderate for kappa =0.4–0.6, and poor for kappa =0–0.2 (27). Linear regressions and Bland-Altman plots were generated to assess the correlation and agreement between 2 observers in the assessment of the extent of pulmonary interstitial fibrosis. The extent of pulmonary interstitial fibrosis assessed with HRCT and 3D UTE were analyzed with Spearman correlation analysis and the Mann-Whitney U test.

Results

Patient characteristics

As shown in *Figure 1*, 36 patients with IPF (34 men and 2 women; mean age: 62±8 years, age range: 43–78 years) were included in this study. The clinical information of all participants is shown in *Table 1*.

Image quality analysis

Interobserver agreements for 3D UTE-MRI, HASTE, and HRCT image quality are shown in *Table 2*. All interobserver agreements were significant and deemed "substantial" (3D UTE-MRI: κ =0.766, P<0.001; HRCT: κ =0.786, P<0.001; HASTE: κ =0.864, P<0.001). As shown in *Figure 2*, the image quality score for 3D UTE-MRI (4.1±0.7) was significantly inferior to that of HRCT (4.9±0.3; P<0.001), although it was higher than that of HASTE (3.0±0.3, P<0.001). The intra-observer agreement for 3D UTE-MRI image quality assessments was deemed "excellent" (κ =0.829; P<0.001).

The feasibility of 3D UTE-MRI

All interobserver agreements to the lung parenchymal findings are shown in *Table 3*. These values were significant and deemed either "substantial" or "excellent" (3D UTE-

Table 1 Clinical characteristics of patients with IPF

Patients	Clinical characteristics
Mean age (years) [range]	62 [43–78]
Gender (female/male), n (%)	2 (5.6)/34 (94.4)
Height (cm)	167.5±6.1
Weight (kg)	71.2±8.5
BMI (kg/m^2)	25.4±2.6
Smoker, n (%)	30 (83.3)
Radiological patterns on HRCT, n (%)	
UIP	30 (83.3)
Possible UIP	6 (16.7)
Pulmonary function tests	
FEV1 % predicted	85.4±14.0
FVC % predicted	83.0±15.5
FEV1/FVC % predicted	81.4±7.3
DLCO % predicted	53.3±11.5
GAP score, n (%)	
I	25 (69.4)
II	10 (27.8)
III	1 (2.8)

IPF, idiopathic pulmonary fibrosis; BMI, body mass index; UIP, usual interstitial pneumonia; FEV, forced expiratory volume; FVC, forced vital capacity; DLCO, diffusing capacity of the lungs for carbon monoxide; GAP, gender-age-physiology variables (FVC and DLCO).

MRI: 0.719≤ κ ≤0.824, P<0.001; HRCT: 0.727≤ κ ≤1, P<0.001; HASTE: 0.654≤ κ ≤1, P<0.001). Inter-method agreements for 3D UTE-MRI and HRCT assessments were significant and deemed "substantial" for the evaluation of reticulation (*vs.* HRCT: κ =0.654; P<0.001), honeycombing (*vs.* HRCT: κ =0.625; P<0.001), and traction bronchiectasis (*vs.* HRCT: κ =0.640; P<0.001), although those for GGOs and emphysema were not significant (P>0.05). On the contrary, inter-method agreements for

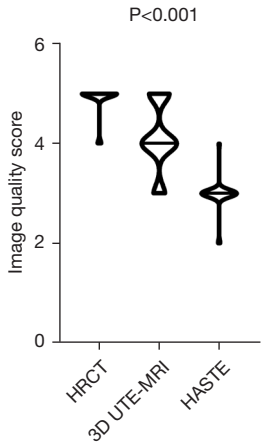

Figure 2 A violin plot graph shows the image quality scores of HRCT, 3D UTE-MRI, and HASTE. Median: the line that crosses the box; data density: smoothed histograms alone the data point. 3D UTE-MRI, 3D ultrashort echo time magnetic resonance imaging; HASTE, half-Fourier single-shot turbo spin-echo; HRCT, high-resolution computed tomography.

Table 2 Interobserver agreement to image quality of HRCT, 3D UTE-MRI, and HASTE

Methods	Investigators	Visual score					Kappa value	P value
		1	2	3	4	5		
HRCT	Reader 1	0	0	0	2	34	0.786	0.001
	Reader 2	0	0	0	3	33		
3D UTE-MRI	Reader 1	0	0	6	20	10	0.766	0.001
	Reader 2	0	0	6	19	11		
HASTE	Reader 1	0	2	32	2	0	0.846	0.001
	Reader 2	0	2	33	1	0		

3D UTE-MRI, 3D ultrashort echo time magnetic resonance imaging; HASTE, half-Fourier single-shot turbo spin-echo; HRCT, high-resolution computed tomography.

Table 3 Interobserver and inter-method agreement when assessing lung parenchymal changes using the HRCT, 3D UTE-MRI, and HASTE

Radiological finding	Methods	Investigators	Visual score		Kappa[a] value	Kappa[b] value	Kappa[c] value
			0	1			
GGO	HRCT	Reader 1	30	6	0.727*	–	–
		Reader 2	29	7			
	UTE	Reader 1	4	32	0.719*	0.017	–
		Reader 2	4	32			
	HASTE	Reader 1	0	36	1	–	0.000
		Reader 2	0	36			
Reticular	HRCT	Reader 1	1	35	1	–	–
		Reader 2	1	35			
	UTE	Reader 1	3	33	0.786*	0.654*	–
		Reader 2	2	34			
	HASTE	Reader 1	14	22	0.880*	–	0.096
		Reader 2	12	24			
Honeycomb	HRCT	Reader 1	5	31	0.893*	–	–
		Reader 2	6	30			
	UTE	Reader 1	14	22	0.818*	0.625*	–
		Reader 2	11	25			
	HASTE	Reader 1	34	2	0.654*	–	0.011
		Reader 2	35	1			
Traction bronchiectasis	HRCT	Reader 1	2	34	1	–	–
		Reader 2	2	34			
	UTE	Reader 1	5	31	0.768*	0.640*	–
		Reader 2	5	31			
	HASTE	Reader 1	12	24	0.816*	–	0.189
		Reader 2	13	23			
Emphysema	HRCT	Reader 1	18	18	0.944*	–	–
		Reader 2	17	19			
	UTE	Reader 1	28	8	0.824*	0.304	–
		Reader 2	30	6			
	HASTE	Reader 1	36	0	1	–	0.000
		Reader 2	36	0			

[a], interobserver agreement between the two readers for HRCT, HASTE, 3D UTE-MRI; [b], intra-method agreement between HRCT and 3D UTE-MRI; [c], intra-method agreement between HRCT and HASTE; *, P<0.001. HRCT, high-resolution computed tomography; 3D UTE-MRI, 3D ultrashort echo time magnetic resonance imaging; HASTE, half-Fourier single-shot turbo spin-echo; GGO, ground-glass opacity.

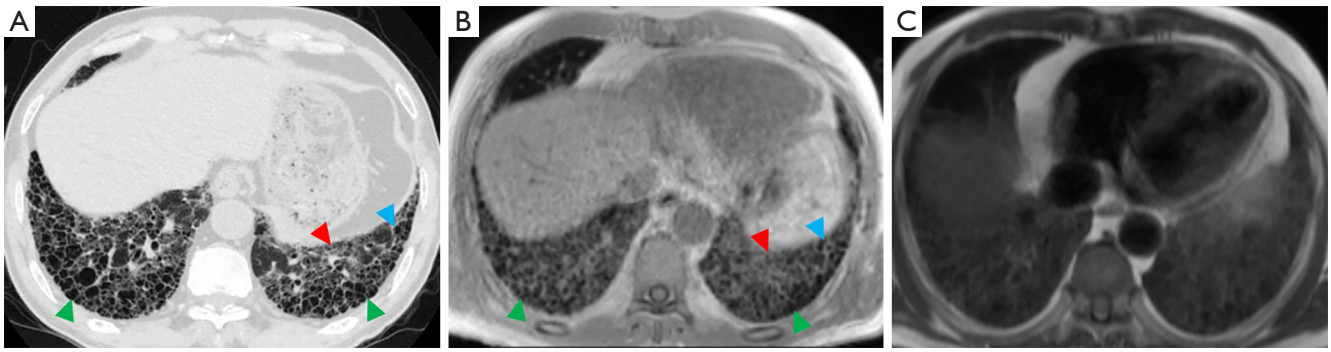

Figure 3 A 77-year-old male patient with interstitial pulmonary fibrosis. Images were obtained with HRCT (A), 3D UTE-MRI (B), and HASTE (C). Honeycombing (green arrow), reticular patterns (red arrow), and traction bronchiectasis (blue arrow) are seen in the left and/or right lower lobes. 3D UTE-MRI and HRCT image qualities are equal (IQS: 5), which were higher than the HASTE image quality (IQS: 4). The extent of pulmonary fibrosis on images obtained with 3D UTE-MRI (IQS: 16) was equal to those obtained with HRCT (IQS: 16). The transverse 3D UTE-MRI images are MPRs. HRCT, high-resolution computed tomography; 3D UTE-MRI, 3D ultrashort echo time magnetic resonance imaging; HASTE, half-Fourier single-shot turbo spin-echo; MPRs, multiplanar reconstructions; IQS, image quality score.

HASTE and HRCT image assessments were deemed "fair" for parenchymal findings. The intra-observer agreement for the lung parenchymal findings on 3D UTE-MRI were significant and deemed either "substantial" or "excellent" when assessing GGO (κ =0.842; P<0.001), reticulation (κ =0.786; P<0.001), honeycombing (κ =0.869; P<0.001), traction bronchiectasis (κ =0.893; P<0.001), and emphysema (κ =0.906; P<0.001).

The diagnostic performance of 3D UTE-MRI in assessment of IPF

Representative imaging features of IPF, including reticulation, traction bronchiectasis, and honeycombing, but not emphysema, could be visualized on 3D UTE-MRI (*Figures 3*,*4*; Figure S1). Using HRCT as the gold standard, the sensitivity and accuracy of 3D UTE-MRI for reticulation (97.1%, 97.2%), honeycombing (83.3%, 86.1%), traction bronchiectasis (94.1%, 94.4%), and emphysema (31.6%, 63.9%) were superior to those of HASTE (SE: reticulation, 65.7%, honeycombing, 3.3%, traction bronchiectasis, 67.6%, emphysema, 0; AC: reticulation, 66.7%, honeycombing, 19.4%, traction bronchiectasis, 69.4%, emphysema, 47.2%). However, the sensitivity of GGOs on 3D UTE-MRI (85.7%) was inferior to that of HASTE (100%). The specificities of reticulation, traction bronchiectasis, honeycombing, and emphysema, but not of GGO, were all 100% on 3D UTE-MRI and HASTE (3D UTE-MRI, 10.3%; HASTE, 0) (*Table 4*).

As indicated in *Table 5*, 3D UTE-MRI had a sensitivity of 97.2% for the detection of pulmonary fibrosis. Only 1 patient with IPF was absent of pulmonary fibrosis on 3D UTE-MRI (Figure S2). The 3D UTE-MRI protocol enabled us to identify 28 (90%) of 31 patients with total fibrosis scores of 6–15 and 2 (40%) of 5 patients with a total fibrosis score >15. *Figure 5* shows high correlations between the 2 readers when elevating the extent of pulmonary fibrosis from both methods (HRCT, R^2=0.84; 3D UTE-MRI, R^2=0.84). The mean difference and 95% limits of agreement (95% LOA) between the 2 readers from HRCT and 3D UTE-MRI were –0.86 (–3.48 to 1.75) and –1.28 (–4.00 to 1.44), respectively. *Figure 6* shows that the extent of pulmonary fibrosis assessed with 3D UTE-MRI (median =9, IQR: 6.25 to 10.00) positively correlated with that from HRCT (median =12, IQR: 9.25 to 13.00) (r=0.72, P<0.001), although the extent of pulmonary interstitial fibrosis assessed with 3D UTE-MRI was lower than that from HRCT (U=320.00, P<0.001; *Figure 7*).

Discussion

In this study, we analyzed the image quality, feasibility, and diagnostic performance of 3D UTE-MRI in the assessment of IPF. Our results indicated that the image quality of 3D UTE-MRI was inferior to that of HRCT, but superior to that of HASTE. The high inter- and intra-observer agreements in the assessment of IPF with 3D UTE-MRI indicated its high feasibility. Moreover, 3D UTE-MRI

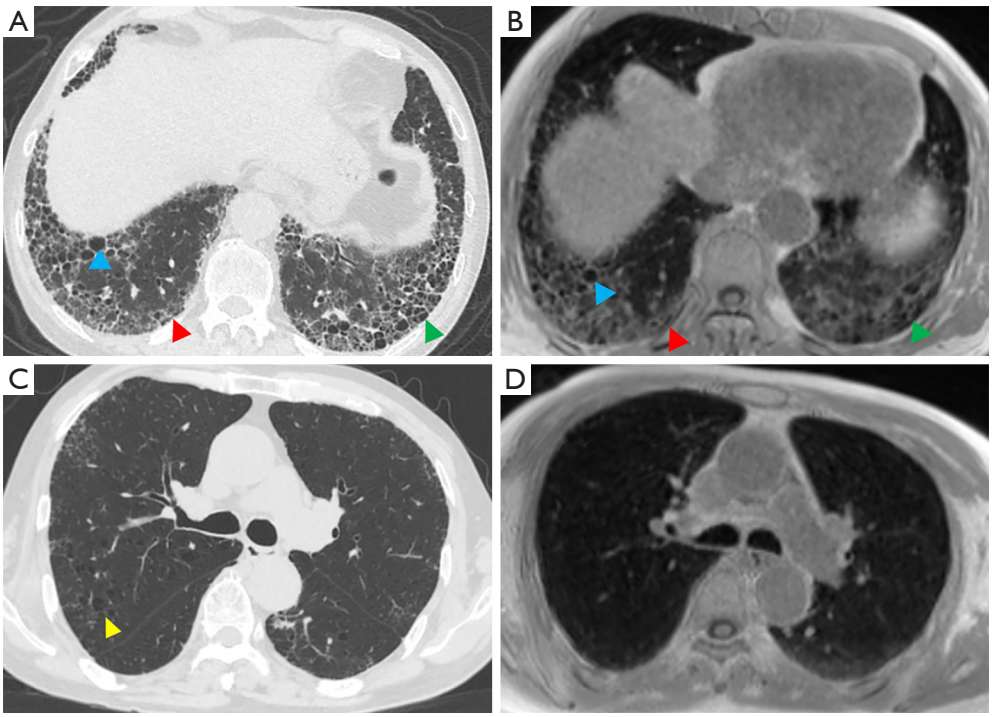

Figure 4 A 68-year-old male patient with interstitial pulmonary fibrosis and emphysema. Images obtained with HRCT (A), and 3D UTE-MRI (B) show honeycombing (green arrow), reticular patterns (red arrow), and traction bronchiectasis (blue arrow) in the left and/or right lower lobes. The image quality of the 3D UTE-MRI (IQS: 4) was lower than that of the HRCT (IQS: 5). The extent of pulmonary fibrosis on images obtained with 3D UTE-MRI (IQS: 10) was lower than those obtained with HRCT (IQS: 14). The images obtained with HRCT also showed that the pulmonary emphysema (yellow arrow) was heterogeneously distributed in the low attenuated areas of both lungs (C). However, pulmonary emphysema was not seen in the lung segments of the 3D UTE-MRI images (D). The transverse 3D UTE-MRI images are MPRs. HRCT, high-resolution computed tomography; 3D UTE-MRI, 3D ultrashort echo time magnetic resonance imaging; IQS, image quality score; MPRs, multiplanar reconstructions.

Table 4 Sensitivity, specificity, and accuracy of 3D UTE-MRI and HASTE for detecting radiologic features

Radiologic features	HRCT, n	3D UTE-MRI				HASTE			
		n	Sensitivity, %	Specificity, %	Accuracy, %	n	Sensitivity, %	Specificity, %	Accuracy, %
GGO	7	32	85.7	10.3	25.0	36	100.0	0.0	19.4
Reticulation	35	34	97.1	100.0	97.2	23	65.7	100.0	66.7
Honeycombing	34	32	83.3	100.0	86.1	1	3.3	100.0	19.4
Traction bronchiectasis	30	25	94.1	100.0	94.4	23	67.6	100.0	69.4
Emphysema	19	6	31.6	100.0	63.9	0	0.0	100.0	47.2

3D UTE-MRI, 3D ultrashort echo time magnetic resonance imaging; HASTE, half-Fourier single-shot turbo spin-echo; HRCT, high-resolution computed tomography; GGO, ground-glass opacity.

Table 5 The sensitivity of 3D UTE-MRI in the assessment of pulmonary fibrosis

Pulmonary fibrosis	HRCT, n	3D UTE-MRI, n	Sensitivity	$R^{2\#}$	$R^{2\&}$
Present	36	35	97%	–	–
Degree*				0.84	0.84
Score 1–5	0	5	–		
Score 6–15	31	28	90%		
Score >15	5	2	40%		

*, degree is based on the sum of scores in six zones (minimum score was 0, the maximum score was 30); #, the correlation between the two readers for HRCT; &, the correlation between the two readers for 3D UTE-MRI. 3D UTE-MRI, 3D ultrashort echo time magnetic resonance imaging; HRCT, high-resolution computed tomography.

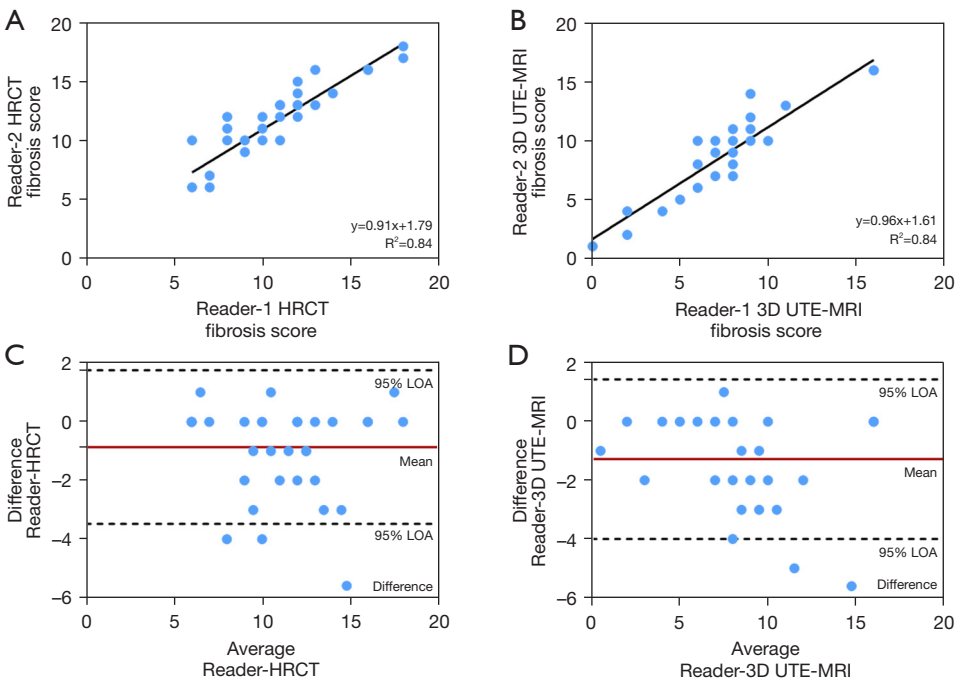

Figure 5 The extent of pulmonary fibrosis obtained with reader one plotted as a function of reader two for IPF patients with both HRCT (R^2=0.84, P<0.001) and 3D UTE-MRI (R^2=0.84, P<0.001) (A,B). Bland-Altman plot of the agreement analysis of the extent of pulmonary fibrosis between reader one and reader two from HRCT and 3D UTE-MRI. Mean difference for HRCT (Reader 1, Reader 2) =0.86, 95% limits of agreement =–3.48 to 1.75 (C). Mean difference for 3D UTE-MRI (Reader 1, Reader 2) =–1.28, 95% limits of agreement =–4.00 to 1.44 (D). IPF, idiopathic pulmonary fibrosis; HRCT, high-resolution computed tomography; 3D UTE-MRI, 3D ultrashort echo time magnetic resonance imaging; LOA, limits of agreement.

presented a high consistency with HRCT in the detection of representative imaging features of IPF, including reticulation, traction bronchiectasis, and honeycombing signs. The extent of pulmonary fibrosis assessed with 3D UTE-MRI was lower than that from HRCT; however, they were positively correlated.

In our research, the image quality of 3D UTE-MRI was inferior to that of HRCT. Consistent with Ohno *et al.* (17), we also found that the image quality of HRCT was superior to that of UTE-MRI. This may have been caused by low SNR, motion corruption, image resolution, and the different gating states of UTE image acquisition, but it could also be the effect of stripes and blurring. We observed minimal artifacts in the upper zones of the lung among

some patients. This may have been because we used NUFT as a reconstruction method, which sometimes generated artifacts in the upper lung areas. There were no significantly blurred images, which may have been related to the gating tolerance and the larger FOV in 3D UTE image acquisition which leads to blurred images at a high level. In our study, the 3D UTE-MRI with improved techniques was used to minimize the motion and enhance the parenchymal signal. However, these techniques still depend on extended acquisition times of several min. As a result, the method remains sensitive to respiratory motion. Moreover, images from 3D UTE-MRI were acquired at end-expiration and HRCT at end-inspiration. This different acquisition phase may affect the discrimination of lung parenchyma imaging features. The image quality of 3D UTE-MRI was superior to that of HASTE, which was the first sequence used for imaging lung parenchymal abnormalities in patients with ILD (3). This suggests that 3D UTE-MRI has the potential to evaluate lung parenchyma structure.

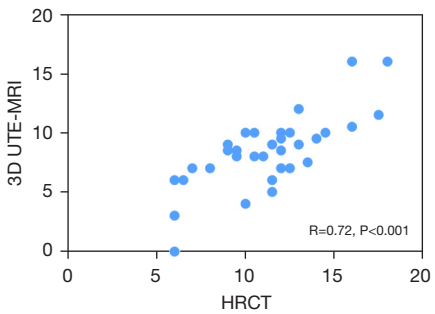

Figure 6 Correlation between the extent of pulmonary fibrosis with HRCT and 3D UTE-MRI (R=0.72, P<0.001). HRCT, high-resolution computed tomography; 3D UTE-MRI, 3D ultrashort echo time magnetic resonance imaging.

The perfect agreements among the 2 radiologists when assessing IPF with 3D UTE-MRI suggested that 3D UTE-MRI images can feasibly be used to assess IPF. The inter-method agreement between 3D UTE-MRI and HRCT was equal to the inter- and intra-observer agreement for 3D UTE-MRI when evaluating the radiologic findings in patients with IPF, especially for traction bronchiectasis, reticular, and honeycomb patterns. Conversely, the inter-method agreement between HASTE and HRCT was poor.

Moreover, the diagnostic performance of 3D UTE-MRI when evaluating honeycombing, reticulation, and traction bronchiectasis of IPF was comparable to that of HRCT and superior to that of HASTE. This was attributed to the improved SNR. The acquisition-weight stack of spiral sequence acquired high-resolution 3D UTE images by using the variable-duration slice encoding to minimize T2 decay, separating slice thickness from in-plane resolution to reduce the number of slice encodings, and using spiral trajectories to accelerate in-plane data collections (20). In addition, the prospective respiratory gating during free-breathing and non-uniform sampling during the readout also provided sufficient SNR and limited artifacts (10). Benlala *et al.* (28) suggested that UTE could be used for emphysema quantification. However, in our study, 3D UTE-MRI showed poorer sensitivity and accuracy when detecting emphysema and GGO compared with HRCT. This finding was similar to that of a previous study (17), that the decreased lung tissue in patients with emphysema will reduce the SNR gains from variable density sampling.

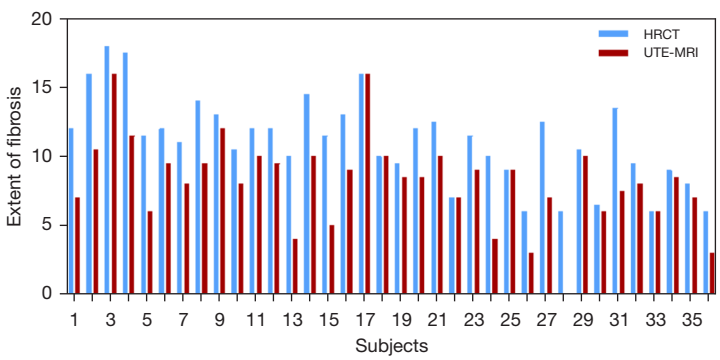

Figure 7 A bar chart showing the discrepancies in the extent of pulmonary fibrosis obtained with an average of two readers between HRCT (blue) and 3D UTE-MRI (red) for 36 patients with IPF. HRCT, high-resolution computed tomography; 3D UTE-MRI, 3D ultrashort echo time magnetic resonance imaging; IPF, idiopathic pulmonary fibrosis.

However, in our research, more GGOs were shown in 3D UTE-MRI than in HRCT. A possible reason for this is that the 3D UTE-MRI were acquired in the expiratory phase during a dynamic free-breathing session and related to the different respiratory phases between the free-breathing 3D UTE-MRI and HRCT. The extent of pulmonary interstitial fibrosis of IPF is helpful in evaluating disease progression and response to treatment. The extent of pulmonary fibrosis measured by 3D UTE-MRI was positively correlated with that measured by HRCT. However, 3D UTE-MRI subtly underestimated the extent of pulmonary fibrosis in comparison with HRCT, which was consistent with a previous study (29). A possible reason for this is that HRCT images were acquired during a static inspiratory breath-hold near total lung capacity, which enabled a better definition of reticulation and honeycombing than was possible with 3D UTE-MRI, which was acquired in the expiratory phase (30). Our results suggested that 3D UTE-MRI was not significantly inferior to HRCT but rather had similar potential to assess the radiologic features of IPF. Apart from that, the most significant advantage of MRI over HRCT is the ability to provide functional information (31-39).

There were several limitations to this study. First, because of the strict inclusion criteria and that most IPF patients were male, only a small number of patients at a single center were included in this research. The predominantly male cohort may limit the generalizability of our findings. Second, we did not set a control group in this study because a previous study suggested that the value of the UTE-MRI imaging method could be reflected by healthy volunteers (19). Third, compared with HRCT, 3D UTE-MRI scans have relatively longer scanning times, which makes them more sensitive to respiratory motion and may influence the imaging quality. Furthermore, 3D UTE-MRI was acquired at end-expiration and HRCT was acquired at end-inspiration, which affected the assessment of imaging quality, imaging patterns. and the extent of fibrosis. The recent development of a temporally resolved low-resolution navigator and a compressed sensing probe, and technical UTE pulse sequence improvements, shows potential to create high-resolution free-breathing pulmonary MRI imaging (40-43). Further technical advances will enable 3D UTE-MRI to provide more functional information and clinical applications.

Conclusions

This study demonstrated that 3D UTE-MRI, a radiation-free non-contrast-enhanced imaging method, can be an alternative to HRCT in the evaluation and follow-up of IPF patients. We found that 3D UTE-MRI has high reproducibility and good performance when identifying imaging features of IPF.

Acknowledgments

Some results of our study have been accepted as an oral presentation at the scientific sessions of the Joint Annual Meeting ISMRM-ESMRMB & ISMRT 31st Annual Meeting, 07–12 May 2022 in London, England, UK.
Funding: This work was supported by the National Key Technologies R & D Program Precision Medicine Research (No. 2021YFC2500700; No. 2016YFC0901101) and the National Natural Science Foundation of China (No. 81870056).

Footnote

Reporting Checklist: The authors have completed the GRRAS reporting checklist. Available at https://qims.amegroups.com/article/view/10.21037/qims-21-1133/rc

Conflicts of Interest: All authors have completed the ICMJE uniform disclosure form (available at https://qims.amegroups.com/article/view/10.21037/qims-21-1133/coif). TB is employed by Siemens Healthcare GmbH and JA is employed by Siemens Shenzhen Magnetic Resonance Ltd. The other authors have no conflicts of interest to declare.

Ethical Statement: The authors are accountable for all aspects of the work in ensuring that questions related to the accuracy or integrity of any part of the work are appropriately investigated and resolved. The study was approved by the Ethics Committee of the China-Japan Friendship Hospital (No. 2019-123-K85-1). The study was conducted in accordance with the Declaration of Helsinki (as revised in 2013). Informed consent was provided by all patients.

References

1. Raghu G, Remy-Jardin M, Myers JL, Richeldi L, Ryerson CJ, Lederer DJ, et al. Diagnosis of Idiopathic Pulmonary Fibrosis. An Official ATS/ERS/JRS/ALAT Clinical Practice Guideline. Am J Respir Crit Care Med 2018;198:e44-68.
2. Ciet P, Tiddens HA, Wielopolski PA, Wild JM, Lee EY, Morana G, Lequin MH. Magnetic resonance imaging in children: common problems and possible solutions for lung and airways imaging. Pediatr Radiol 2015;45:1901-15.
3. Hatabu H, Gaa J, Tadamura E, Edinburgh KJ, Stock KW, Garpestad E, Edelman RR. MR imaging of pulmonary parenchyma with a half-Fourier single-shot turbo spin-echo (HASTE) sequence. Eur J Radiol 1999;29:152-9.
4. Puderbach M, Eichinger M, Gahr J, Ley S, Tuengerthal S, Schmähl A, Fink C, Plathow C, Wiebel M, Müller FM, Kauczor HU. Proton MRI appearance of cystic fibrosis: comparison to CT. Eur Radiol 2007;17:716-24.
5. Puderbach M, Eichinger M, Haeselbarth J, Ley S, Kopp-Schneider A, Tuengerthal S, Schmaehl A, Fink C, Plathow C, Wiebel M, Demirakca S, Müller FM, Kauczor HU. Assessment of morphological MRI for pulmonary changes in cystic fibrosis (CF) patients: comparison to thin-section CT and chest x-ray. Invest Radiol 2007;42:715-25.
6. Hekimoğlu K, Sancak T, Tor M, Beşir H, Kalaycioğlu B, Gündoğdu S. Fast MRI evaluation of pulmonary progressive massive fibrosis with VIBE and HASTE sequences: comparison with CT. Diagn Interv Radiol 2010;16:30-7.
7. Rajaram S, Swift AJ, Capener D, Telfer A, Davies C, Hill C, Condliffe R, Elliot C, Hurdman J, Kiely DG, Wild JM. Lung morphology assessment with balanced steady-state free precession MR imaging compared with CT. Radiology 2012;263:569-77.
8. Benlala I, Albat A, Blanchard E, Macey J, Raherison C, Benkert T, Berger P, Laurent F, Dournes G. Quantification of MRI T2 Interstitial Lung Disease Signal-Intensity Volume in Idiopathic Pulmonary Fibrosis: A Pilot Study. J Magn Reson Imaging 2021;53:1500-7.
9. Ohno Y, Nishio M, Koyama H, Takenaka D, Takahashi M, Yoshikawa T, Matsumoto S, Obara M, van Cauteren M, Sugimura K. Pulmonary MR imaging with ultra-short TEs: utility for disease severity assessment of connective tissue disease patients. Eur J Radiol 2013;82:1359-65.
10. Johnson KM, Fain SB, Schiebler ML, Nagle S. Optimized 3D ultrashort echo time pulmonary MRI. Magn Reson Med 2013;70:1241-50.
11. Ohno Y, Nishio M, Koyama H, Yoshikawa T, Matsumoto S, Seki S, Obara M, van Cauteren M, Takahashi M, Sugimura K. Pulmonary 3 T MRI with ultrashort TEs: influence of ultrashort echo time interval on pulmonary functional and clinical stage assessments of smokers. J Magn Reson Imaging 2014;39:988-97.
12. Bauman G, Johnson KM, Bell LC, Velikina JV, Samsonov AA, Nagle SK, Fain SB. Three-dimensional pulmonary perfusion MRI with radial ultrashort echo time and spatial-temporal constrained reconstruction. Magn Reson Med 2015;73:555-64.
13. Dournes G, Grodzki D, Macey J, Girodet PO, Fayon M, Chateil JF, Montaudon M, Berger P, Laurent F. Quiet Submillimeter MR Imaging of the Lung Is Feasible with a PETRA Sequence at 1.5 T. Radiology 2015;276:258-65.
14. Roach DJ, Crémillieux Y, Fleck RJ, Brody AS, Serai SD, Szczesniak RD, Kerlakian S, Clancy JP, Woods JC. Ultrashort Echo-Time Magnetic Resonance Imaging Is a Sensitive Method for the Evaluation of Early Cystic Fibrosis Lung Disease. Ann Am Thorac Soc 2016;13:1923-31.
15. Higano NS, Hahn AD, Tkach JA, Cao X, Walkup LL, Thomen RP, Merhar SL, Kingma PS, Fain SB, Woods JC. Retrospective respiratory self-gating and removal of bulk motion in pulmonary UTE MRI of neonates and adults. Magn Reson Med 2017;77:1284-95.
16. Geiger J, Zeimpekis KG, Jung A, Moeller A, Kellenberger CJ. Clinical application of ultrashort echo-time MRI for lung pathologies in children. Clin Radiol 2021;76:708.e9-708.e17.
17. Ohno Y, Koyama H, Yoshikawa T, Seki S, Takenaka D, Yui M, Lu A, Miyazaki M, Sugimura K. Pulmonary high-resolution ultrashort TE MR imaging: Comparison with thin-section standard- and low-dose computed tomography for the assessment of pulmonary parenchyma diseases. J Magn Reson Imaging 2016;43:512-32.
18. Romei C, Turturici L, Tavanti L, Miedema J, Fiorini S, Marletta M, Wielopolski P, Tiddens H, Falaschi F, Ciet P. The use of chest magnetic resonance imaging in interstitial lung disease: a systematic review. Eur Respir Rev 2018;27:180062.
19. Dournes G, Yazbek J, Benhassen W, Benlala I, Blanchard E, Truchetet ME, Macey J, Berger P, Laurent F. 3D ultrashort echo time MRI of the lung using stack-of-spirals and spherical k-Space coverages: Evaluation in healthy

volunteers and parenchymal diseases. J Magn Reson Imaging 2018;48:1489-97.
20. Qian Y, Boada FE. Acquisition-weighted stack of spirals for fast high-resolution three-dimensional ultra-short echo time MR imaging. Magn Reson Med 2008;60:135-45.
21. Dale B, Wendt M, Duerk JL. A rapid look-up table method for reconstructing MR images from arbitrary K-space trajectories. IEEE Trans Med Imaging 2001;20:207-17.
22. Hausmann D, Niemann T, Kreul D, Nocito A, Klarhöfer M, Nickel DM, Kiefer B, Attenberger UI, Zöllner FG, Kubik-Huch RA. Free-Breathing Dynamic Contrast-Enhanced Imaging of the Upper Abdomen Using a Cartesian Compressed-Sensing Sequence With Hard-Gated and Motion-State-Resolved Reconstruction. Invest Radiol 2019;54:728-36.
23. Gay SE, Kazerooni EA, Toews GB, Lynch JP 3rd, Gross BH, Cascade PN, Spizarny DL, Flint A, Schork MA, Whyte RI, Popovich J, Hyzy R, Martinez FJ. Idiopathic pulmonary fibrosis: predicting response to therapy and survival. Am J Respir Crit Care Med 1998;157:1063-72.
24. Lynch DA, Sverzellati N, Travis WD, Brown KK, Colby TV, Galvin JR, Goldin JG, Hansell DM, Inoue Y, Johkoh T, Nicholson AG, Knight SL, Raoof S, Richeldi L, Ryerson CJ, Ryu JH, Wells AU. Diagnostic criteria for idiopathic pulmonary fibrosis: a Fleischner Society White Paper. Lancet Respir Med 2018;6:138-53.
25. Müller NL, Mayo JR, Zwirewich CV. Value of MR imaging in the evaluation of chronic infiltrative lung diseases: comparison with CT. AJR Am J Roentgenol 1992;158:1205-9.
26. Best AC, Meng J, Lynch AM, Bozic CM, Miller D, Grunwald GK, Lynch DA. Idiopathic pulmonary fibrosis: physiologic tests, quantitative CT indexes, and CT visual scores as predictors of mortality. Radiology 2008;246:935-40.
27. Mandrekar JN. Measures of interrater agreement. J Thorac Oncol 2011;6:6-7.
28. Benlala I, Berger P, Girodet PO, Dromer C, Macey J, Laurent F, Dournes G. Automated Volumetric Quantification of Emphysema Severity by Using Ultrashort Echo Time MRI: Validation in Participants with Chronic Obstructive Pulmonary Disease. Radiology 2019;292:216-25.
29. Pinal-Fernandez I, Pineda-Sanchez V, Pallisa-Nuñez E, Simeon-Aznar CP, Selva-O'Callaghan A, Fonollosa-Pla V, Vilardell-Tarres M. Fast 1.5 T chest MRI for the assessment of interstitial lung disease extent secondary to systemic sclerosis. Clin Rheumatol 2016;35:2339-45.
30. Gruden JF. CT in Idiopathic Pulmonary Fibrosis: Diagnosis and Beyond. AJR Am J Roentgenol 2016;206:495-507.
31. Marinelli JP, Levin DL, Vassallo R, Carter RE, Hubmayr RD, Ehman RL, McGee KP. Quantitative assessment of lung stiffness in patients with interstitial lung disease using MR elastography. J Magn Reson Imaging 2017;46:365-74.
32. Gargani L, Bruni C, De Marchi D, Romei C, Guiducci S, Bellando-Randone S, Aquaro GD, Pepe A, Neri E, Colagrande S, Falaschi F, Moggi-Pignone A, Pingitore A, Matucci-Cerinic M. Lung magnetic resonance imaging in systemic sclerosis: a new promising approach to evaluate pulmonary involvement and progression. Clin Rheumatol 2021;40:1903-12.
33. Buzan MT, Eichinger M, Kreuter M, Kauczor HU, Herth FJ, Warth A, Pop CM, Heussel CP, Dinkel J. T2 mapping of CT remodelling patterns in interstitial lung disease. Eur Radiol 2015;25:3167-74.
34. Lederlin M, Bauman G, Eichinger M, Dinkel J, Brault M, Biederer J, Puderbach M. Functional MRI using Fourier decomposition of lung signal: reproducibility of ventilation- and perfusion-weighted imaging in healthy volunteers. Eur J Radiol 2013;82:1015-22.
35. Harlaar L, Ciet P, van Tulder G, Pittaro A, van Kooten HA, van der Beek NAME, Brusse E, Wielopolski PA, de Bruijne M, van der Ploeg AT, Tiddens HAWM, van Doorn PA. Chest MRI to diagnose early diaphragmatic weakness in Pompe disease. Orphanet J Rare Dis 2021;16:21.
36. Mummy DG, Bier EA, Wang Z, Korzekwinski J, Morrison L, Barkauskas C, McAdams HP, Tighe RM, Driehuys B, Mammarappallil JG. Hyperpolarized 129Xe MRI and Spectroscopy of Gas-Exchange Abnormalities in Nonspecific Interstitial Pneumonia. Radiology 2021;301:211-20.
37. Wang JM, Robertson SH, Wang Z, He M, Virgincar RS, Schrank GM, Smigla RM, O'Riordan TG, Sundy J, Ebner L, Rackley CR, McAdams P, Driehuys B. Using hyperpolarized 129Xe MRI to quantify regional gas transfer in idiopathic pulmonary fibrosis. Thorax 2018;73:21-8.
38. Ohno Y, Nishio M, Koyama H, Yoshikawa T, Matsumoto S, Seki S, Tsubakimoto M, Sugimura K. Oxygen-enhanced MRI for patients with connective tissue diseases: comparison with thin-section CT of capability for pulmonary functional and disease severity assessment. Eur J Radiol 2014;83:391-7.
39. Heidenreich JF, Weng AM, Metz C, Benkert T, Pfeuffer J, Hebestreit H, Bley TA, Köstler H, Veldhoen S.

Three-dimensional Ultrashort Echo Time MRI for Functional Lung Imaging in Cystic Fibrosis. Radiology 2020;296:191-9.
40. Jiang W, Ong F, Johnson KM, Nagle SK, Hope TA, Lustig M, Larson PEZ. Motion robust high resolution 3D free-breathing pulmonary MRI using dynamic 3D image self-navigator. Magn Reson Med 2018;79:2954-67.
41. Johnson KM. Hybrid radial-cones trajectory for accelerated MRI. Magn Reson Med 2017;77:1068-81.
42. Zhu X, Chan M, Lustig M, Johnson KM, Larson PEZ. Iterative motion-compensation reconstruction ultra-short TE (iMoCo UTE) for high-resolution free-breathing pulmonary MRI. Magn Reson Med 2020;83:1208-21.
43. Ong F, Zhu X, Cheng JY, Johnson KM, Larson PEZ, Vasanawala SS, Lustig M. Extreme MRI: Large-scale volumetric dynamic imaging from continuous non-gated acquisitions. Magn Reson Med 2020;84:1763-80.

Cite this article as: Yang X, Liu M, Duan J, Sun H, An J, Benkert T, Dai H, Wang C. Three-dimensional ultrashort echo time magnetic resonance imaging in assessment of idiopathic pulmonary fibrosis, in comparison with high-resolution computed tomography. Quant Imaging Med Surg 2022;12(8):4176-4189. doi: 10.21037/qims-21-1133

